REPULSIVE CORE POTENTIAL AND ELASTIC HEAVY-ION COLLISIONS

V.YU. DENISOV, O.I. DAVIDOVSKAYA

Institute for Nuclear Research, Nat. Acad. of Sci. of Ukraine
(47, Prosp. Nauky, Kyiv 03680, Ukraine)

UDC 539.14

Within the optical model with a repulsive core, the elastic collisions of $^{16}O+^{12}C$ at various energies are discussed. Due to the repulsive core, the cross-sections rise strongly for backward angles. By using the near-side/far-side decomposition method, it is shown that the near-side component of the scattering amplitude mainly contributes to the elastic scattering cross-sections for forward and backward angles. The repulsive core of the $^{16}O+^{12}C$ potential occurs at small distances.

1. Introduction

The nucleus-nucleus interaction potential is a key ingredient in the analysis of nuclear reactions. By using the potential between nuclei, we can evaluate the cross sections of different nuclear reactions [1–5].

The interaction potential between nuclei consists of nuclear, Coulomb, and centrifugal parts. The Coulomb and centrifugal interactions of two nuclei are well-known. In contrast to this, the nuclear part of a nucleus-nucleus interaction is known worse. There are various approximations for the nuclear part of the nucleus-nucleus interaction potential.

The nuclear part of the interaction potential is often parametrized by the Woods–Saxon, squared Woods–Saxon, or similar shapes [1–7] which is the very common phenomenological approach. Parameters of the phenomenological potential are obtained by fitting the experimental data for various reactions. Therefore, the parameters of such a potential depend on the reaction channel(s) and the model applied to the reaction description.

There are several macroscopic, semimicroscopic, and microscopic approaches for the evaluation of the nucleus-nucleus potential [4, 5]. The proximity potential is derived in the framework of the macroscopic approximation using the properties of nuclear matter, nuclear surface, density distributions in nuclei, and simple nucleon-nucleon interaction [8]. There are various semimicroscopic and microscopic models of the nucleus-nucleus potential based on the Skyrme nucleon-nucleon forces [9–15,17] or a simplified energy-density functional [16, 17]. Note that various properties of nuclear matter and nuclei are well described in the frameworks of the Hartree–Fock or energy-density functional theories with the Skyrme forces. The microscopic double-folding nucleus-nucleus potential is based on the M3Y, Paris, or Reid nucleon-nucleon forces and nucleon densities of both nuclei [4, 5, 18–28]. The microscopic single-folding nucleus-nucleus potential is also used for description of heavy-ion reactions [1, 4, 5, 29].

The Woods–Saxon type, single-, and double-folding [4, 5, 18–22, 24] potentials are steadily rise from a large negative value at $R = 0$ with increasing the distance R between nuclei. The nuclear part of these potentials is attractive at any distances between nuclei. In contrast to this, the proximity potential [8], the potentials based on the Skyrme [9–13, 15], the modified M3Y [25–27], and the Reid soft-core [28] effective nucleon-nucleon forces are attractive at large and close distances between interacting nuclei and are repulsive at very small distances, when nuclei are strongly overlapped. The potentials based on the simplified energy-density functional [16, 17] have also the repulsive core at very small distances. In other words, there is the repulsive core at very small distances and the attraction at larger distances for the proximity, Skyrme-type, modified M3Y, and Reid soft-core potentials [8–13, 15–17, 25–27].

The core-repulsive nucleus-nucleus potential was discussed in [16] for the first time. The repulsion of two colliding nuclei takes place at small distances, when the densities of two nuclei are well overlapped and doubled in some volume. The compressibility of nuclear matter resists to such high value of nuclear density [11, 16]. The kinetic energy contribution into the nucleus-nucleus interaction rises sharply due to the Pauli rearrangement and the antisymmetrization as well [9, 28]. The both compressibility and kinetic energy contributions into the nucleus-nucleus potential are directly taken into account in the framework of semimicroscopical models based on the Skyrme effective energy density functional [9–12, 15].

The obvious example clarifying the nature of a repulsive core of the nucleus-nucleus potential is the

potential evaluated at frozen nucleon densities for fully overlapped colliding nuclei, when the distance between the nucleus-nucleus mass centers R is zero. In this case, the density in the inner part of the overlapped nuclei is twice higher than the normal density of nuclear matter. Such high-density state of nuclear matter is unstable; therefore, a local or absolute minimum of the potential at $R = 0$ cannot exist. Therefore, the result of potential evaluations based on the Skyrme force and frozen nucleon densities leading to the core at $R = 0$ is expected. In contrast to this, the microscopic double-folding nucleus-nucleus potentials based on the M3Y, Paris, or Reid nucleon-nucleon forces and frozen nucleon densities have the absolute minimum at $R = 0$ [4,18–22, 24]. The values of such double-folding nucleus-nucleus potentials at $R = 0$ belong to the range $-150 \div -400$ MeV. Note that the accounting of the nuclear three-body force leads to a reduction of the potential depth at $R = 0$ in the framework of the double-folding approach [31] by 20–30%. The origin of the strong attraction of two nuclei at $R = 0$ is doubtful.

The most part of experimental data for various nucleus-nucleus reactions have been analyzed using the Woods–Saxon type and double-folding potentials [1–7, 18–24, 31]. However, only few reactions and potential properties have been considered with the use of the potentials with a repulsive core [9–16, 25–28, 30]. Therefore, it is very interesting to analyze various reactions employing the potential with a repulsive core.

The repulsion of colliding nuclei exists at small distances between them. Therefore, the influence of the repulsive core on scattering properties can be checked in reactions which are very sensitive to values of the potential at small distances. The elastic-scattering reaction involving very stiff nuclei ^{16}O and ^{12}C at energies strongly above the barrier seems to be a reasonable example, because this reaction is very sensitive to the potential values at small distances [21, 22, 24].

The ^{16}O+^{12}C elastic scattering data at several energies strongly above the barrier were measured by Ogloblin *et al.* [21, 22]. These data have been described by using the very deep double-folding and Woods–Saxon potentials in [21, 22]. A shallow potential evaluated from a single-folding method was obtained in [29] for these reaction data sets. The ^{16}O+^{12}C elastic scattering data were recently analyzed by using a parabolic ℓ-dependent core [30]. However, the nucleus-nucleus potential is attractive at the core distances (see [30]). Therefore, it is very interesting to describe this reaction data using the repulsive core potential, whose type is very similar to the Skyrme semimicroscopic potential.

In the second section of the work, we briefly discuss the parametrization of a phenomenological interaction potential with a repulsive core. The discussion of the results and the conclusion are given in Section 3.

2. Potential Parametrization

The real part of the nucleus-nucleus potential $v(R)$ consists of the Coulomb $v_{\rm C}(R)$, nuclear $v_{\rm n}(R)$, and centrifugal $v_\ell(R)$ parts, i.e.

$$v(R) = v_{\rm C}(R) + v_{\rm n}(R) + v_\ell(R). \tag{1}$$

These parts of the nucleus-nucleus potential can be written in the form

$$v_{\rm C}(R) = \begin{cases} \dfrac{Z_1 Z_2 e^2}{R}, & \text{if } R \geq R_C, \\ \dfrac{Z_1 Z_2 e^2}{R_C}\left[\dfrac{3}{2} - \dfrac{R^2}{2R_C^2}\right], & \text{if } R < R_C, \end{cases} \tag{2}$$

$$v_{\rm n}(R) = \\ = \begin{cases} \dfrac{-V_0}{1+\exp[(R - r_0(A_1^{1/3} + A_2^{1/3}))/d_0]}, & \text{if } R \geq R_m, \\ b_0 + b_1 s + b_2 s^2 + b_3 s^3 + b_4 s^4, & \text{if } R < R_m, \end{cases} \tag{3}$$

$$v_\ell(R) = \frac{\hbar^2 \ell(\ell+1)}{2M[A_1 A_2/(A_1 + A_2)]R^2}. \tag{4}$$

Here, $A_{1,2}$ and $Z_{1,2}$ are, respectively, the number of nucleons and the number of protons in corresponding nuclei, e is the proton charge, M is the nucleon mass, $R_C = r_C(A_1^{1/3} + A_2^{1/3})$, $s = R - R_m$, and ℓ is the orbital momentum. As discussed in Introduction, the repulsion part of the potential is related to both the compressibility of nuclear matter and the kinetic energy contribution due to the Pauli rearrangement and the antisymmetrization. This repulsion appears at small distances between the approaching nuclei, when the densities of the colliding nuclei strongly overlapped and overcome the equilibrium density of nuclear matter in some volume. Therefore, the potential form, see Eqs. (3), is different for different distances between the nuclei.

The nuclear part of the potential and the derivative of the potential should be continuous at the matching point R_m. Therefore,

$$b_0 = \frac{-V_0}{1+\exp[(R_m - r_0(A_1^{1/3} + A_2^{1/3}))/d_0]}, \tag{5}$$

$$b_1 = \frac{V_0 \exp[(R_m - r_0(A_1^{1/3} + A_2^{1/3}))/d_0]}{d_0\{1 + \exp[(R_m - r_0(A_1^{1/3} + A_2^{1/3}))/d_0]\}^2}. \quad (6)$$

The semimicroscopic potential [10–12] between heavy nuclei is evaluated in the frozen-density approximation at the center-to-center distance R as

$$V(R) = \int d\mathbf{r}\, \varepsilon[\rho_{1p}(\mathbf{r}) + \rho_{2p}(R,\mathbf{r}), \rho_{1n}(\mathbf{r}) + \rho_{2n}(R,\mathbf{r})] -$$

$$- \int d\mathbf{r}\, \varepsilon[\rho_{1p}(\mathbf{r}), \rho_{1n}(\mathbf{r})] - \int d\mathbf{r}\, \varepsilon[\rho_{2p}(\mathbf{r}), \rho_{2n}(\mathbf{r})]. \quad (7)$$

Here, $\varepsilon[\rho_{ip}(\mathbf{r}), \rho_{in}(\mathbf{r})]$ is the total Skyrme SkM* energy-density functional which includes all $\hbar^2$ correction terms in the kinetic energy density functional obtained in the extended Thomas–Fermi approximation, and $\rho_{ip}(\mathbf{r})$ and $\rho_{in}(\mathbf{r})$ are, respectively, the proton and neutron Hartree–Fock–BCS densities of the i-th nucleus ($i = 1, 2$). The first term in Eq. (7) is the energy of the interacting nuclei at a finite distance R, while the other ones are the energies of the non-interacting nuclei. An analytic expression for the semimicroscopic potential was derived by fitting the calculated semimicroscopic potentials for 7140 reactions for various projectile and target nuclei between ^{16}O and ^{212}Po [10]. The barrier heights evaluated by using the analytic expression for the semimicroscopic potential are well reproduced by experimental data especially for light nuclei [10, 33]. Moreover, the analytic expression for the nucleus-nucleus potential well fits the semimicroscopic potentials for a lot of colliding ions and in a wide range of distances between them. The four-power polynomial is successfully used in [10] for the parametrization of the nuclear part of the potential at small distances between nuclei. Therefore, we choose the polynomial behavior of the nuclear part of the potential at distances $R < R_m$, see Eq. (3).

The imaginary part of the nucleus-nucleus potential consists of the volume and surface parts, i.e.

$$W(R) = -\frac{W_0}{1 + \exp[(R - r_w(A_1^{1/3} + A_2^{1/3}))/d_w]} -$$

$$- \frac{W_s \exp[(R - r_s(A_1^{1/3} + A_2^{1/3}))/d_s]}{d_s\{1 + \exp[(R - r_s(A_1^{1/3} + A_2^{1/3}))/d_s]\}^2}. \quad (8)$$

Such a representation of the imaginary potential is common in the theory of nucleus-nucleus collisions [1, 4, 5].

If 14 parameters V_0, r_0, d_0, b_2, b_3, b_4, R_m, R_C, W_0, r_w, d_w,W_s, r_s, and d_s are known, then we can describe the angular distribution of a nuclear reaction in the framework of the optical model. Former 8 and latter 6 parameters are related to the real and imaginary parts of the potential, respectively.

3. Results and Discussions

3.1. Elastic scattering

We find 14 parameters of the potential by fitting the data for the ^{16}O+^{12}C elastic scattering. For each collision energy, we search the parameter set, which lead to the least

$$\chi^2 = \frac{1}{N}\sum_{i=1}^{N} \frac{(\sigma_{\rm calc}(\theta_i) - \sigma_{\rm exp}(\theta_i))^2}{\delta\sigma_{\rm exp}(\theta_i)}.$$

Here, N is the number of experimental points, $\sigma_{\rm calc}(\theta_i)$ and $\sigma_{\rm exp}(\theta_i)$ are, respectively, the theoretical and experimental values of the cross-section at the angle θ_i, and $\delta\sigma_{\rm exp}(\theta_i)$ is the corresponding error. To increase the weight of the data points at large angles, which are especially sensitive to the strength and shape of the optical potential at small distances, we have assumed, as in [22], $\delta\sigma_{\rm exp}(\theta_i) = 0.1\sigma_{\rm exp}(\theta_i)$ for all data points. The scattering data are known at ^{16}O beam energies of 132 [21, 22], 169, 200, 230, 260 [22], and 181 MeV [34]. The evaluated sets of potential parameters are given in Table 1.

Optical potential parameter sets used for the system ^{16}O+^{12}C

$E_{\rm lab}$(MeV)	132	169	181	200	230	260
V_0(MeV)	37.258	39.092	39.089	46.426	92.948	41.585
r_0(fm)	0.967	1.048	1.094	1.063	1.012	1.066
d_0(fm)	0.851	0.761	0.796	0.736	0.354	0.763
b_2(MeV fm^{-2})	–3.721	–3.132	–3.475	–1.271	–5.263	–3.721
b_3(MeV fm^{-3})	6.391	5.854	5.664	5.103	–4.519	4.897
b_4(MeV fm^{-4})	1.850	2.232	1.632	1.442	–0.319	1.692
R_m(fm)	6.341	5.717	6.169	6.343	5.697	6.235
R_c(fm)	4.946	6.123	5.188	6.029	10.791	5.689
W(MeV)	15.009	18.302	18.090	19.960	8.242	45.616
r_w(fm)	1.104	1.102	1.170	1.168	1.285	0.919
d_w(fm)	0.337	0.366	0.322	0.381	0.292	0.297
W_s(MeV)	7.634	10.109	8.150	5.950	36.493	18.231
r_s(fm)	1.313	1.278	1.253	1.263	1.031	1.155
d_s(fm)	0.388	0.436	0.515	0.507	0.712	0.522
σ^a(mb)	1327	1399	1474	1409	1451	1422
χ^2	16.2	16.3	21.2	15.0	10.1	5.5

[a] The total reaction cross section.

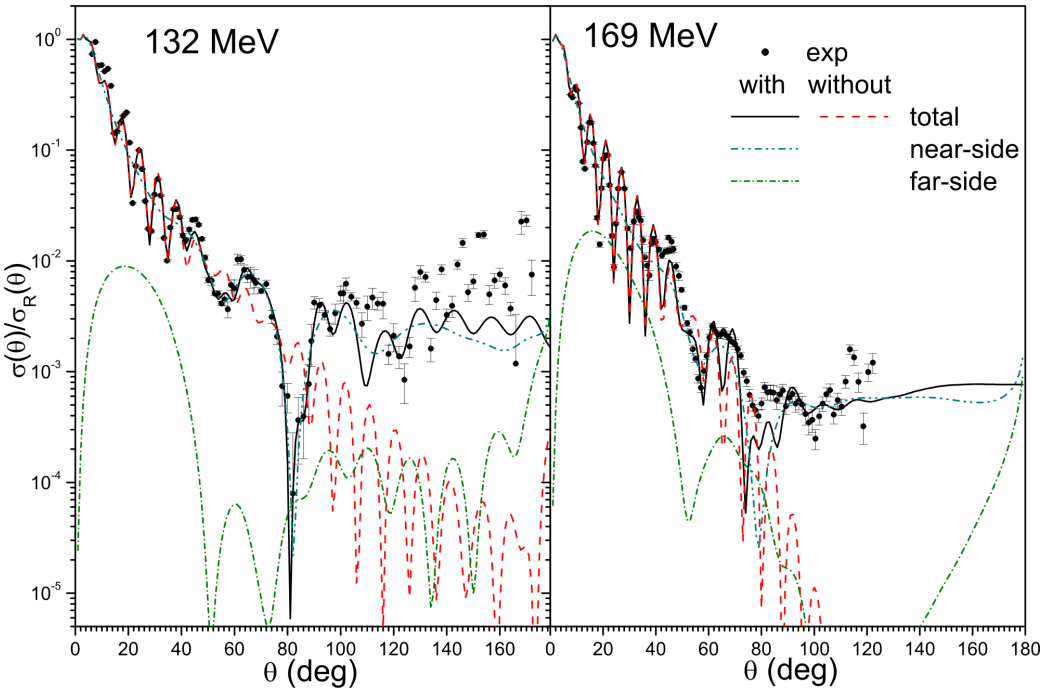

Fig. 1. Elastic-scattering data and optical model calculations for potentials with and without a repulsive core for $E_{\rm cm}$=132 MeV (left panel) and $E_{\rm cm}$=169 MeV (right panel). The cross-sections for total and near-side/far-side decompositions of the elastic ^{16}O+^{12}C scattering amplitude evaluated with a repulsive core in the potential

Figures 1–3 show the data and the optical model fits obtained by the repulsive core potentials for various energies. The parameters of these potentials are listed in Table 1. The repulsive core nucleus-nucleus potentials (1)–(6) for $\ell = 0$ with parameters from Table 1 at various collision energies are shown in Fig. 4. These potentials have core and well at small distances, see Fig. 4. Note that the bottom of the well $V_{\rm well}$, which takes place at distance $R_{\rm well}$, is the lowest value of the potential.

To demonstrate the repulsive core effect, we show the results of calculations obtained within the optical model with potentials without core in Figs. 1–3. The coreless potential for such calculations coincides with the corresponding repulsive core potential at distances $R \geq R_{\rm well}$ and equals $V_{\rm well}$ at $R \leq R_{\rm well}$. The optical model calculations for such coreless potential are presented by dashed lines in Figs. 1–3. We clearly see the influence of the repulsive core by comparing the results in Figs. 1-3. Due to the inner repulsion, the cross-section increases drastically at backward angles. In contrast to this, the values of cross-sections at forward angles are very similar for the both types of potentials.

The value of χ^2 evaluated with the repulsive core potential (see Table 1) for an energy of 132 MeV is lower than that in [22] and higher than that in [30]. (Note that our approach to the evaluation of χ^2 is the same as in [22] and different from that in [30].) However, we obtain slightly larger values of χ^2 for collision energies other than those in [22, 30]. So, the description quality obtained in our model is similar to that in [22, 30]. In contrast to this, the values of χ^2 presented in [29] are much larger than the corresponding ones in Table 1 or in [22]. Note that the elastic ^{16}O+^{12}C scattering data for a beam energy of 181 MeV have not been discussed in [21, 22, 29].

The forward-angle cross-sections evaluated using the strongly attractive nucleus-nucleus potentials show the prominent Fraunhofer diffraction structure with very deep and narrow dips, see Figs. in [21, 22]. In contrast to this, the dips of the forward-angle cross-sections obtained in our approach are shallow. Our values of the cross-sections in these dips are located close to the experimental data in contrast those in [21, 22]. The Fraunhofer diffraction structure with very deep and narrow dips at forward angles contradicts the data.

The values of the total cross section presented in Table 1 are close to the corresponding ones in [22]. Note that the inner core has no effect on the total cross section.

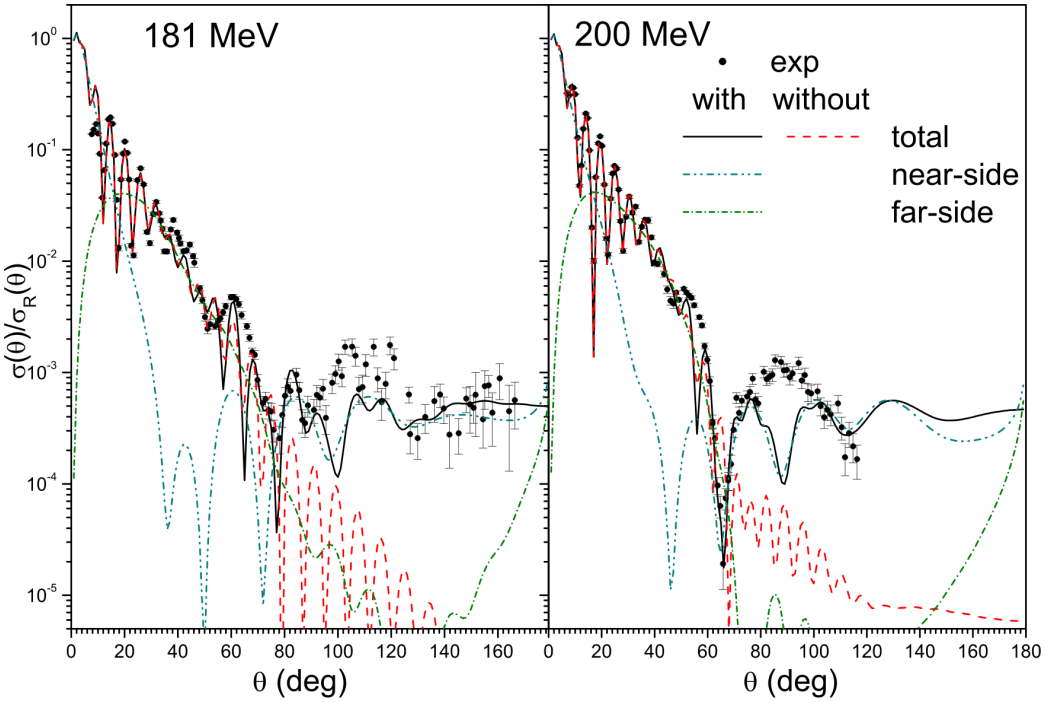

Fig. 2. The same as in Fig. 1, but for $E_{\rm cm}$=181 MeV (left panel) and $E_{\rm cm}$=200 MeV (right panel)

3.2. Potentials

The repulsive-core nucleus-nucleus potentials (1)-(6) for $\ell = 0$ with parameters from Table 1 at various collision energies are compared with the proximity [8] and semimicroscopic [10] potentials in Fig. 4.

The depth of a capture well depends on the collision energy for the repulsive core potential.

The semimicroscopic potential evaluated by using the Skyrme SkM* energy-density functional [see Eq. (7)], which takes into account all $\hbar^2$ correction terms in the kinetic energy density functional and frozen proton and neutron Hartree–Fock–BCS densities of both nuclei, is presented in Fig. 4. For reference, the semimicroscopic potential calculated by using the approximate expression [10] is also given in Fig. 4. Both semimicroscopic potentials are close to each other. The values of phenomenological repulsive core potentials defined by the elastic scattering are near to the semimicroscopic ones at small distances and around the barrier (see Fig. 4). The depth of a capture well for the semimicroscopic potential is smaller than that for the phenomenological potentials with a repulsive core. The proximity potential [8] and repulsive core potentials are close to each other at small distances, while the proximity potential is too attractive at large distances between nuclei. (Note that the semimicroscopic and proximity potentials are mainly applied to the interaction of two heavy or very heavy nuclei; therefore, we may compare only a global tendency of various potentials.)

The semimacroscopic potential and the repulsive core potentials obtained at various collision energies lead to close values of the barrier heights. Moreover, the values of capture well depths obtained for various collision energies are also close at $R \approx 3 \div 4$ fm. The prominent repulsive core exists at distances $R \lesssim 2.5$ fm for any potential presented in Fig. 4. Therefore, the distances, where the densities of colliding nuclei are well overlapped, and, as a result, the compressibility of nuclear matter [30], Pauli rearrangement, and antisymmetrization lead to a strong repulsion, are the same for all potentials. The core radius evaluated in [30] is approximately $1.5 \div 2$ fm. Note that the nucleus-nucleus potential shape considered in [30] is different from our one which is described by Eqs. (1)–(6) and presented in Fig. 4.

The depths of the potentials evaluated in [22] for various energies belong to the range 170-362 MeV. Therefore, the phenomenological repulsive core potentials (see Fig. 4) are much shallow than those obtained in [22]. The incorporation of the Pauli principle into the the double-folding potentials based on the effective in-medium nucleon-nucleon interaction slightly

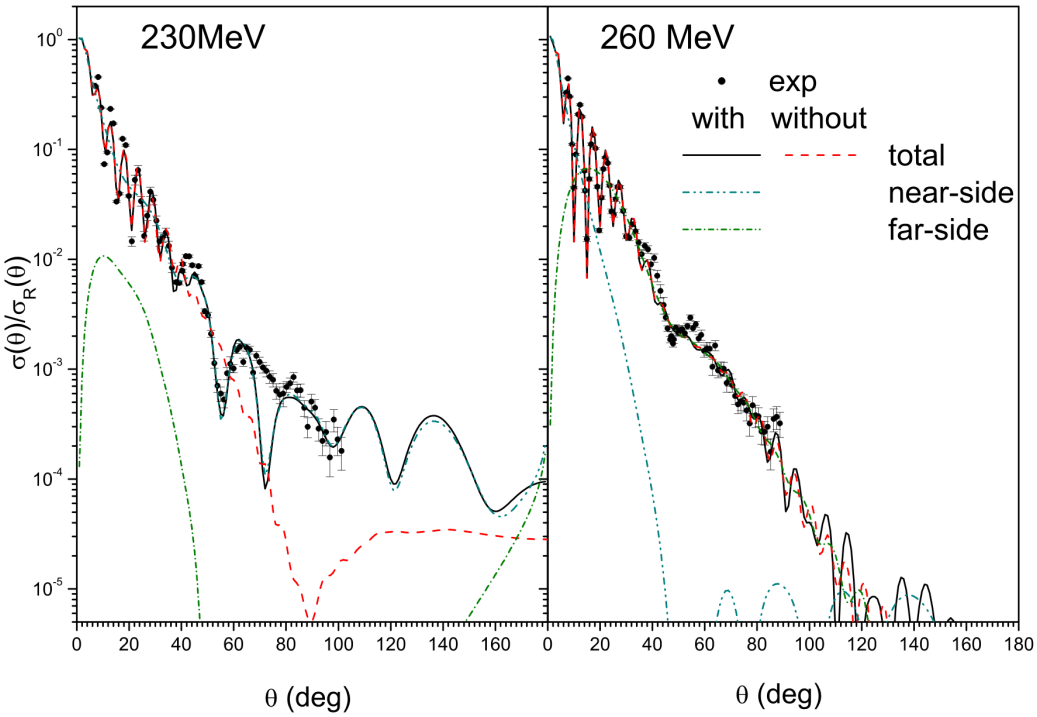

Fig. 3. The same as in Fig. 1, but for $E_{\rm cm}$=230 MeV (left panel) and $E_{\rm cm}$=260 MeV (right panel)

reduces the double-folding potential depth [23, 28]. However, the potentials evaluated by using the Skyrme energy-density functional and various modified M3Y density-dependent nucleon-nucleon forces are very different at small distances.

For the nuclear system formed in a nucleus-nucleus collision at $R = 0$, the lowest value is taken by the energy of a nucleus formed in the fusion of these nuclei in the ground state $E_{\rm fus}$. Using Eq. (7), we find that the minimal value of the nucleus-nucleus potential at $R = 0$ is

$$V(R=0) \geq E_{\rm fus} - E_1 - E_2 = V_{\rm min}(R=0) = -Q_{\rm fus}, \tag{9}$$

where E_i is the energy of the i-th nucleus, and $Q_{\rm fus}$ is the Q-value of the fusion reaction. Taking the experimental evaluation of the ground-state atomic masses into account [35], we obtain $V_{\rm min}(R=0) = -16.75$ MeV for system ^{16}O+^{12}C. Due to this, the very deep attractive potential for this system at $R = 0$ is questionable as pointed in Introduction.

The total energy density functional consists of two terms

$$\varepsilon[\rho_p(\mathbf{r}), \rho_n(\mathbf{r})] = \tau[\rho_p(\mathbf{r}), \rho_n(\mathbf{r})] + \nu[\rho_p(\mathbf{r}), \rho_n(\mathbf{r})]. \tag{10}$$

Here, $\tau[\rho_p(\mathbf{r}), \rho_n(\mathbf{r})]$ is the kinetic energy density functional obtained in the extended Thomas–Fermi approximation which takes into account $\hbar^2$ correction terms, $\nu[\rho_p(\mathbf{r}), \rho_n(\mathbf{r})]$ is the potential part of the total energy-density functional which is related to the nucleon-nucleon force.

Substituting Eq. (10) into (7), we can present the nucleus-nucleus potential as the sum of two terms

$$V(R) = V_T(R) + V_{NN}(R), \tag{11}$$

where

$$V_T(R) = \int d\mathbf{r}\tau[\rho_{1p}(\mathbf{r}) + \rho_{2p}(R,\mathbf{r}), \rho_{1n}(\mathbf{r}) + \rho_{2n}(R,\mathbf{r})] -$$

$$- \int d\mathbf{r}\ \tau[\rho_{1p}(\mathbf{r}), \rho_{1n}(\mathbf{r})] - \int d\mathbf{r}\ \tau[\rho_{2p}(\mathbf{r}), \rho_{2n}(\mathbf{r})] \tag{12}$$

$$V_{NN}(R) = \int d\mathbf{r}\nu[\rho_{1p}(\mathbf{r}) + \rho_{2p}(R,\mathbf{r}), \rho_{1n}(\mathbf{r}) + \rho_{2n}(R,\mathbf{r})] -$$

$$- \int d\mathbf{r}\ \nu[\rho_{1p}(\mathbf{r}), \rho_{1n}(\mathbf{r})] - \int d\mathbf{r}\ \nu[\rho_{2p}(\mathbf{r}), \rho_{2n}(\mathbf{r})] \tag{13}$$

are the kinetic energy $V_T(R)$ and the nucleon-nucleon force $V_{NN}(R)$ contributions to the nucleus-nucleus potential.

Note that the Skyrme force is a zero-range effective force. Therefore, $V_{NN}(R)$ is related to the single-folding expression. If we use the finite-range effective force $v(\mathbf{r}, \mathbf{r}')$, then $V_{NN}(R)$ is presented as the double-folding expression

$$V_{NN}(R) = \int d\mathbf{r} \int d\mathbf{r}' \; \rho_1(\mathbf{r}) v(\mathbf{r}, \mathbf{r}') \rho_2(R, \mathbf{r}') \qquad (14)$$

which is widely used [1–5, 18–22, 24–28, 31]. We stress that the kinetic energy contribution to the potential $V_T(R)$ is omitted in the evaluation of the double-folding potential in [21, 22, 24, 31]. Examples of interaction potentials between various nuclei evaluated by taking the kinetic energy contribution into account are given in [10–12, 15, 37] and in Fig. 4 (see the results obtained in the semimicroscopic or HF–BCS–SkM* approaches). These potentials have core at small distances, in contrast to the double-folding potentials from [21, 22, 24, 31].

3.3. Near- and far-side cross section decomposition

The near-side/far-side decomposition technique [36] has proven to be of great help in decomposing the interference caused by trajectories originating from different sides of the scattering potential. The convention states that the trajectories being scattered into the same side from whence they came belong to the near-side, whereas the trajectories scattered to the opposite side of the target are the far-side ones [36].

It is shown in [21, 22] by using Fuller's method [36] that the $^{16}O+^{12}C$ elastic scattering cross-section for forward angles is related to the near-side component, while the cross-section for large and back angles is determined by the far-side component. The far-side component is related to the rainbow phenomenon [24] which is related to the refraction of an incident wave by the strongly attractive (very deep) nucleus-nucleus potential. Many other interesting features connected to the near-side/far-side decomposition in the case of a very deep nucleus-nucleus potential are also discussed in [21, 22, 24].

We present the near-side/far-side decomposition of the elastic $^{16}O+^{12}C$ scattering amplitude in Figs. 1–3 which is evaluated, by using the repulsive core potentials.

Figures 1–3 show that, for ^{16}O beam energies of 132, 169, and 230 MeV, the near-side component mainly describes the cross-section in the full range of angles, while the far-side component is responsible only for the fine oscillation structure due to the interference between near- and far-side components. In contrast to this, the near-side component mainly describes the cross-section for forward and backward angles for projectile energies of 181, 200, and 260 MeV, while the far-side component contributes essentially at the angles $30° \div 60°$ for energies of 181 and 200 MeV and at the angles $30° \div 100°$ for an energy of 260 MeV.

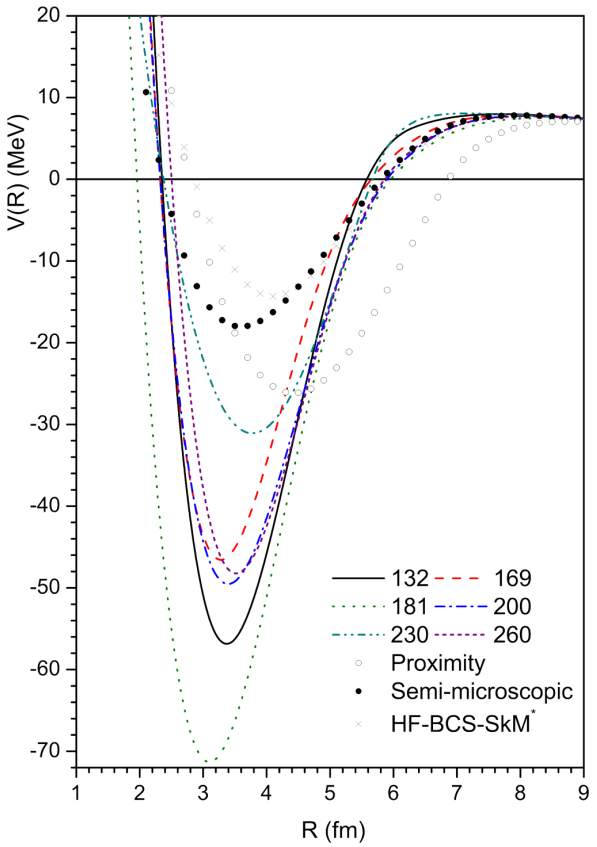

Fig. 4. Potential with a repulsive core evaluated for the elastic $^{16}O+^{12}C$ scattering for ^{16}O beam energies of 132, 169, 181, 200, 230, and 260 MeV. For reference, the proximity [8], semimicroscopic [10] and semimicroscopic HF-BCS-SkM* potentials are presented as well

Due to the repulsive core, both near- and far-side components strongly rise at backward angles.

The repulsive core and coreless potentials are very shallow in comparison with the deep attractive nucleus-nucleus potentials from [21, 22, 24]. Therefore, the rainbow scattering is impossible in our case. However, we are able to describe the scattering data by using the shallow potentials with a repulsive core.

In conclusion, we show that:
– It is possible to describe the elastic scattering data by using the shallow phenomenological potential with a repulsive core.
– The cross-section, as well as both near- and far-side cross-section components, at backward angles are strongly enhanced by the repulsive core.
– The high-energy elastic ^{16}O+^{12}C scattering data show that the repulsive core of a nucleus-nucleus potential takes place at distances $R \lesssim 2.5$ fm.
– The description of the elastic ^{16}O+^{12}C scattering data in the framework of the simple double-folding potential [21, 22] is doubtful, because the kinetic energy contribution to the nucleus-nucleus potential is neglected, and the potential at $R = 0$ is deeper than the lowest possible value $-Q_{\rm fus}$, see Eq. (9).

The authors thank sincerely Dr. A.S. Dem'yanova for sending to us all the data on the ^{16}O+^{12}C elastic scattering used in this paper and Profs. A.A. Ogloblin and W.H. Trzaska for their help in getting the data.

1. P.E. Hodgson, *Nuclear Heavy-Ion Reactions* (Clarendon Press, Oxford 1978).
2. R. Bass, *Nuclear Reactions with Heavy Ions* (Springer, Berlin 1980).
3. W. Nörenberg, H.A. Weidenmüller, *Introduction to the Theory of Heavy-Ion Collisions* (Springer, Berlin 1980).
4. G.R. Satchler, *Direct Nuclear Reactions* (Oxford University Press, Oxford, 1983).
5. P. Frobrich and R. Lipperheide, *Theory of Nuclear Reactions* (Clarendon Press, Oxford, 1996).
6. A. Winther, Nucl. Phys. A **594**, 203 (1995).
7. K. Siwek-Wilczyńska, J. Wilczyński, Phys. Rev. **C69**, 024611 (2004).
8. J. Blocki, J. Randrup, W.J. Swiatecki, and C.F. Tang, Ann. Phys. (N.Y.) **105**, 427 (1977).
9. D.M. Brink and F. Stancu, Nucl. Phys. A **270**, 236 (1976); F. Stancu and D.M. Brink, Nucl. Phys. A **299**, 321 (1978).
10. V.Yu. Denisov, Phys. Lett. B **526**, 315 (2002).
11. V.Yu. Denisov and W. Nörenberg, Eur. Phys. J. A **15**, 375 (2002); V.Yu. Denisov, Eur. Phys. J. A **25**, Suppl. 1, 619 (2005).
12. V.Yu. Denisov and V.A. Nesterov, Phys. Atom. Nucl. **69**, 1472 (2006); Yad. Fiz. **69**, 1507 (2006).
13. V.Yu. Denisov and N.A. Pilipenko, Phys. Rev. C **76**, 014602 (2007).
14. J. Skalski, Acta Phys. Polonica B **34** 1977 (2003); Int. J. Modern Phys. E **13**, 305 (2004).
15. Min Liu, Ning Wang, Zhuxia Li, Xizhen Wu, and Enguang Zhao, Nucl. Phys. A **768**, 80 (2006).
16. K.A. Brueckner, J.R. Buchler, and M.M. Kelly, Phys. Rev. **173**, 944 (1969).
17. C. Ngo, B. Tamain, J. Galin, M. Beiner, and R.J. Lombard, Nucl. Phys. A **240**, 353 (1975); H. Ngo and Ch. Ngo, Nucl. Phys. A **348**, 140 (1980).
18. G. Bertsch, J. Borysowicz, H. McManus, and W.G. Love, Nucl. Phys. A **284**, 399 (1977); N. Anantaraman, H. Toki, and G. Bertsch, Nucl. Phys. A **398**, 269 (1983).
19. G.R. Satchler and W.G. Love, Phys. Rep. **55**, 183 (1979).
20. M.E. Brandan and G.R. Satchler, Phys. Rep. **285**, 143 (1997).
21. A.A. Ogloblin, Dao T. Khoa, Y. Kondo, Yu.A. Glukhov, A.S. Dem'yanova, M.V. Rozhkov, G.R. Satchler, S.A. Goncharov, Phys. Rev. C **57**, 1797 (1998).
22. A.A. Ogloblin, Yu.A. Glukhov, W.H. Trzaska, A.S. Dem'yanova, S.A. Goncharov, R. Julin, S.V. Klebnikov, M. Mutterer, M.V. Rozhkov, V.P. Rudakov, G.P. Tiorin, Dao T. Khoa, and G.R. Satchler, Phys. Rev. C **62**, 044601 (2000).
23. V.B. Soubbotin, W. von Oertzen, X. Vinas, K.A. Gridnev, and H.G. Bohlen, Phys. Rev. C **64**, 014601 (2001); K.A. Gridnev, V.B. Soubbotin, W. von Oertzen, H.G. Bohlen, and X. Vinas, Phys. At. Nucl. **65**, 707 (2002); Yad. Fiz. **65**, 739 (2002).
24. Dao T. Khoa, W. von Oertzen, H.G. Bohlen, and S. Ohkubo, J. Phys. G **34**, R111 (2007).
25. E. Uegaki and Y. Abe, Prog. Theor. Phys. **90**, 615 (1990).
26. S. Misicu and W. Greiner, Phys. Rev. C **69**, 054601 (2004).
27. S. Misicu and H. Esbensen, Phys. Rev. Lett. **96**, 112701 (2006).
28. T. Izumoto, S. Krewald, and A. Faessler, Nucl. Phys. A **341**, 319 (1980); **357**, 487 (1981).
29. S. Hossain, M.N.A. Abdullah, K.M. Hasan, M. Asaduzzaman, M.A.R. Akanda, S.K. Das, A.S.B. Tariq, M.A. Uddin, A.K. Basak, S. Ali, and F.B. Malik, Phys. Lett. B **636**, 248 (2006).
30. K.A. Gridnev, E.E. Rodionova, and S.N. Fadeev, Phys. of Atomic Nucl. **71** 1262 (2008).
31. T. Furumoto, Y. Sakuragi, and Y. Yamamoto, Phys. Rev. C **79**, 011601 (2009).
32. V.Yu. Denisov, O.I. Davidovskaya, *Proc. of 2 Int. Conf. "Current Problems in Nuclear Physics and Atomic Energy"(NPAE-Kyiv2008)*, June 9–15, 2008, Kyiv, Ukraine, to be published.
33. J.O. Newton, R.D. Butt, M. Dasgupta, D.J. Hinde, I.I. Gontchar, C.R. Morton, and K. Hagino, Phys. Rev. C **70**, 024605 (2004).
34. A.S. Dem'yanova, private communication.
35. G. Audi, O. Bersillon, J. Blachot, and A.H. Wapstra, Nucl. Phys. A **729**, 3 (2003).
36. R.C. Fuller, Phys. Rev. C **12**, 1561 (1975).
37. V.Yu. Denisov and V.A. Nesterov, *Proc. of 2 Int. Conf. "Current Problems in Nuclear Physics and Atomic Energy"(NPAE-Kyiv2008)*, June 9–15, 2008, Kyiv, Ukraine, to be published.

ПОТЕНЦІАЛ З ВІДШТОВХУВАЛЬНИМ КОРОМ ТА ПРУЖНІ ЗІТКНЕННЯ ВАЖКИХ ІОНІВ

В.Ю. Денисов, О.І. Давидовська

Р е з ю м е

В рамках оптичної моделі з потенціалом із відштовхувальним кором розглядаються пружні зіткнення $^{16}O+^{12}C$ при різних енергіях. Поперечний переріз на задніх кутах сильно збільшується завдяки відштовхувальному кору. Використовуючи метод розкладу на ближню і дальню компоненти, показано, що ближня компонента амплітуди розсіяння головним чином дає внесок в поперечний переріз пружного розсіяння на передніх і задніх кутах. Відштовхувальний кор $^{16}O+^{12}C$ потенціала має місце на малих відстанях.